High-pressure investigations on the semi-Heusler compound CuMnSb

Pallavi Malavi,[1] Jing Song,[1] Wenli Bi,[2,3] Alexander Regnat,[4] Linghan Zhu,[1] Andreas Bauer,[4] Anatoliy Senyshyn,[5] Li Yang,[1] Christian Pfleiderer,[4] and James S. Schilling[1,*]

[1]*Department of Physics, Washington University, St. Louis, Missouri 63130, USA*
[2]*Argonne National Laboratory, Argonne, Illinois 60439, USA*
[3]*Department of Geology, University of Illinois at Urbana-Champaign, Urbana, Illinois 61801, USA*
[4]*Department of Physics, Technical University Munich, D-85748 Garching, Germany*
[5]*Heinz Maier-Leibnitz Center, Technical University Munich, D-85748 Garching, Germany*

(Received 16 February 2018; revised manuscript received 4 June 2018; published 28 August 2018)

The antiferromagnetic semi-Heusler compound CuMnSb has been investigated under high pressure by electrical resistivity and angle dispersive synchrotron x-ray diffraction measurements to 53 and 36 GPa, respectively. The Néel temperature at ∼50 K is found to initially increase rapidly with pressure, reaching 83 K at 7 GPa. However, near 8 GPa at ambient temperature a sluggish first-order structural transition begins from a semimetallic cubic phase to a likely semimetallic tetragonal phase; thermal cycling to 355 °C at 9.6 GPa serves to complete the transition. In the tetragonal phase no sign of magnetic ordering is visible in the resistivity $R(T)$ over the measured temperature range 4–295 K. This suggests that magnetic ordering may have shifted to temperatures well above ambient. Indeed, density functional calculations find the magnetic ground state in the tetragonal phase to be antiferromagnetic. Following decompression to 1 bar at ambient temperature, the high-pressure tetragonal phase is retained.

DOI: 10.1103/PhysRevB.98.054431

I. INTRODUCTION

Heusler compounds form an intensively studied class of magnetic materials exhibiting novel physical properties due to strong spin polarization of charge carriers at the Fermi level, high Curie temperatures and martensite structural transitions, with possible application to spintronics and magnetic shape-memory devices [1]. Although a large number of ferromagnetic (FM) half-metals have been discovered in the cubic-structured full and semi-Heusler class, antiferromagnetism is quite rare in this family.

NiMnSb and PtMnSb are examples of half-metallic ferromagnets with Curie temperatures well above room temperature [2,3], reaching values over 700 K [4]. These semi-Heusler compounds crystallize in the cubic $C1_b$-type semi-Heusler structure (space group $F\bar{4}3m$) consisting of three filled and one vacant interpenetrating fcc sublattices. CuMnSb is isostructural to NiMnSb and PtMnSb and is so far known to be the only example of an antiferromagnetic (AFM) Mn-based member among the semi-Heusler compounds based on 3d transition metals [5]. Below the Néel temperature, $T_N \approx 50$ K, CuMnSb develops commensurate magnetic order in which FM planes of ordered Mn moments along the ⟨111⟩ direction couple antiferromagnetically [6]. Recent transport, magnetization, and neutron scattering results on phase-pure single crystals of CuMnSb reveal a second anomaly at 34 K that results from a canting of the commensurate AFM structure without net magnetic moment [7]. Despite the structural similarities to half-metallic semi-Heusler compounds, density functional studies by Jeong *et al.* [8] suggest that CuMnSb is a self-doped compensated semimetal and not a half-metal. The AFM phase in CuMnSb is particularly interesting due to its large ordered Mn moments, hallmarks of both local moment–itinerant magnetism, and the stability of magnetic order to high magnetic fields [9–11].

The physical properties of semi-Heusler compounds are found to be very sensitive to disorder and various structural defects due to empty sites that arise during the sample synthesis [12]. In fact, a detailed model calculation by Máca *et al.* [13] shows that the experimentally observed AFM 111 phase in CuMnSb is not the magnetic ground state but is stabilized by defects such as Mn antisites on the Cu sublattice, Mn interstitials, and possibly Cu-Mn intermixing. The vacant sublattice in the crystal structure makes this system susceptible to external perturbations such as pressure or doping. Both of these parameters influence the Fermi surface and the hybridization between different orbitals, thereby affecting all physical properties.

Several doping-dependent studies have been performed on CuMnSb to reveal the role played by the nonmagnetic 3d- and sp-electron atoms on the magnetic properties. Substitution of Cu by Ni (Pt) leads to a linear decrease (increase) of the lattice constant whereby strong ferromagnetism is established for very small doping concentrations [14–16]. Also, detailed first-principle calculations on Co/Ni-doped CuMnSb and CuMnZ (Z = In, Sn, Sb, Te) reveal that the magnetic exchange interactions in these compounds can be described in terms of competition between the ferromagnetic Ruderman-Kittel-Kasuya-Yosida (RKKY) -type exchange and antiferromagnetic superexchange, depending on the relative positions of the unoccupied minority Mn 3d states and the Fermi level [17–19]. It would be interesting to study how pressure can tune these parameters in a relatively well-defined manner and thereby influence the unusual AFM state in CuMnSb.

*Corresponding author: jss@wuphys.wustl.edu

There exist several theoretical studies on Heusler compounds that explore the pressure dependence of the magnetic properties [20,21]. Recent theoretical work on IrMnSb predicts a half-metallic transition under pressure due to a shift of the Fermi level in the minority-spin energy gap [22]. Several experimental studies on the variation of the Curie temperature under pressure for Ni-Mn-based systems have been reported [4,23–27]. Apart from these, there are very few high-pressure studies on the semi-Heusler systems, especially with regard to the changes in the crystal structure or transport properties.

The relatively low magnetic ordering temperature in CuMnSb is believed to be due to the presence of frustration in the magnetic interaction that arises since the cubic structure is unfavorable for robust antiferromagnetism [28]. However, in low-symmetry structures, a large enhancement of T_N is predicted theoretically in CuMnP and observed experimentally in bulk (orthorhombic) as well as thin films (tetragonal) of CuMnAs [28,29]. The tetragonal structure of CuMnAs has recently attracted considerable experimental and theoretical attention as a favorable candidate for applications in AFM spintronics [29,30] due to its high Néel temperature. Lowering symmetry from cubic to tetragonal/orthorhombic is believed to enhance the magnetocrystalline anisotropy that relieves the frustration in the nearest-neighbor magnetic coupling. This can result in values of T_N far above room temperature.

CuMnSb would appear to be the ideal case to study whether pressure can generate the necessary structural distortions to relieve the magnetic frustration by lowering the crystal symmetry. With this motivation we have studied the transport and structural properties of CuMnSb under pressure. The cubic $C1_b$ structure is found to be stable up to ~7 GPa with pressure favoring AFM ordering in this phase stability region, as evidenced from the enhanced Néel temperature. The temperature dependence of resistance shows dramatic changes above 7 GPa presumably at least in part due to disorder-induced localization associated with a sluggish first-order structural transition to a lower symmetry structure (CuMnAs-like tetragonal phase). In this high-pressure phase no evidence for magnetic ordering is observed in the present resistivity measurements below 300 K, suggesting that the ordering temperature may have shifted to temperatures well above ambient.

II. EXPERIMENTAL DETAILS

For the present study, tiny phase-pure samples of CuMnSb were prepared from ingots float-zoned in an ultrahigh vacuum compatible image furnace [31–33]. Polycrystalline samples from the beginning of the growth process were selected, i.e., before grain selection has taken place. For details on the crystal growth process and the metallurgical characterization, we refer to Ref. [7].

High pressures were generated in a diamond anvil cell (DAC) made of CuBe alloy [34] by two opposing diamond anvils (1/6 carat, type Ia) with 0.5-mm-diameter culets. The rhenium gasket (6–7 mm diameter, 250 μm thick) was preindented to 75 μm and a 260-μm-diameter hole electrospark drilled through the center. The center section of the preindented gasket surface was filled with a 4:1 cubic-boron-nitride (cBN)-epoxy mixture to insulate the gasket and serve as nonhydrostatic pressure medium. Four thin (4-μm-thick) Pt strips made

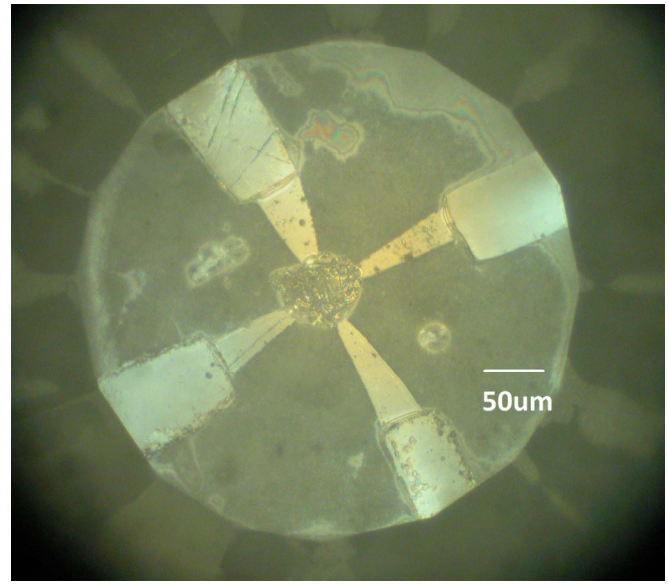

FIG. 1. Image of CuMnSb polycrystalline sample in center resting on four flat (4 μm) Pt leads on insulated Re gasket. Ruby spheres are located at 4 and 10 o'clock from the sample and serve as *in situ* manometers.

electrical contact to the sample (approximate dimensions 50 × 50 × 10 μm^3) (see Fig. 1). Four-point dc electrical resistance measurements with 1 mA excitation current (Keithley 220 current source) were carried out and sample voltages measured by a Keithley 182 nanovoltmeter. Temperature was determined by a calibrated Cernox resistor positioned just above one of the diamond anvils. Several small ruby spheres were placed near the sample to serve as internal manometers [35] over the measured temperature range 4–295 K. In a separate experiment the pressure gradient across a 500 μm culet was measured to allow a small correction of ruby pressure to sample pressure. For example, the ruby pressure of 8.8 GPa was corrected to 9.3 GPa at the sample. A He-gas-driven membrane allowed changes in pressure at cryogenic temperatures provided by a custom-built Oxford flow cryostat. Further details of the pressure techniques used for the electrical resistivity measurements were published earlier [36,37].

High-pressure x-ray diffraction (XRD) measurements at and above room temperature were carried out at the 16-BM-D beamline of the Advanced Photon Source at the Argonne National Laboratory employing a 30 keV monochromatic x-ray beam ($\lambda = 0.4133$ Å). A membrane-driven symmetric DAC with cBN seats was used to allow large angle (2-θ) access. XRD measurements were performed using 350 μm culet diamond anvils and a rhenium gasket with a 175 μm hole filled with CuMnSb powder and neon as pressure transmitting medium. In the room-temperature XRD measurement, pressures were measured *in situ* by the ruby fluorescence method [35]. In a subsequent experiment the temperature range was extended to 355 °C by resistively heating the DAC; a separate piece of gold (~30 μm) was loaded in the gasket hole next to the sample as a pressure marker [38]. Clean spectra from the sample could be collected free of Au peaks. Angle dispersive diffraction patterns were collected using an area detector (Mar345) with an

exposure time of 60–180 s. Two-dimensional x-ray diffraction images were integrated using FIT2Dsoftware [39] and refined with the EXPGUI/GSAS software to extract structural parameters [40].

III. RESULTS

A. Resistance measurements

Figure 2 shows the high-pressure resistance data $R(T)$ up to 53 GPa over the temperature range 4–300 K. For pressures to 6.7 GPa, $R(T)$ exhibits a weakly sublinear temperature dependence upon cooling followed by a pronounced drop or knee that indicates the onset of magnetic ordering, as found in previous resistivity, magnetic susceptibility, and specific heat studies on CuMnSb at ambient pressure [7,10,41]. The resistivity knee arises from the sudden decrease in the spin-disorder scattering when magnetic order sets in. In the present measurements the knee in $R(T)$ is broadened by the pressure gradient across the sample arising from the nonhydrostatic pressure. In this pressure range $R(T)$ shows metallic or semimetallic behavior, the latter indicated by the density functional calculations of Joeng *et al.* [8]. Above 6.7 GPa the knee in $R(T)$ suddenly disappears, $R(T)$ showing instead a small negative slope over the entire temperature range that becomes mildly positive at higher pressures. As pressure is released, a shallow resistivity minimum appears. The sudden change in the temperature-dependent resistance $R(T)$ near 8 GPa signals a possible first-order structural phase transition.

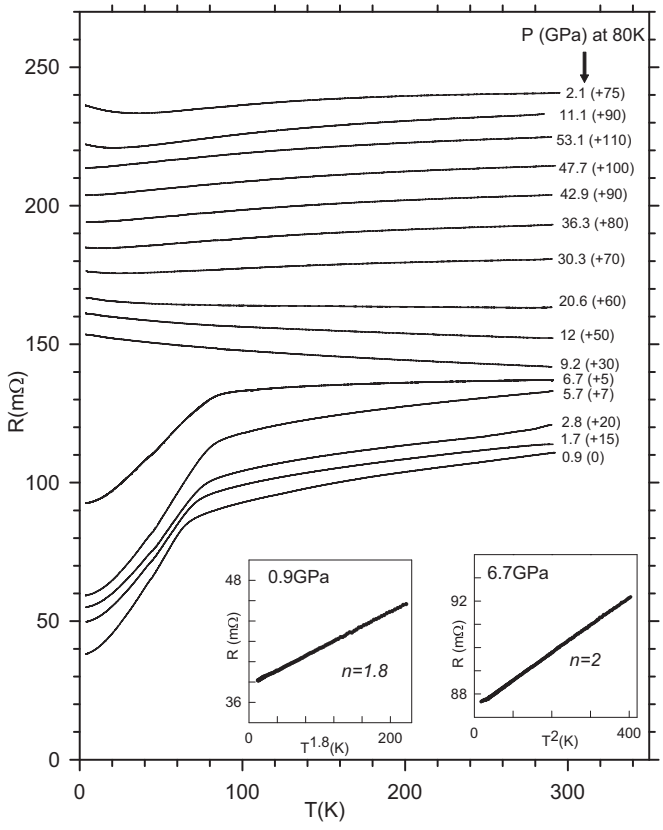

FIG. 2. Four-point resistance of CuMnSb vs temperature at various pressures. Order of measurement is bottom to top. Resistance values apply for measurement at 0.9 GPa; all other data are shifted vertically for clarity by values in mΩ given in parentheses. Insets at the bottom show the temperature dependence of resistance at 0.9 and 6.7 GPa described by power law $R(T) = R_o + AT^n$.

Since the $R(T)$ data in Fig. 2 have been shifted vertically to avoid extensive crossing, the actual measured values of the resistance at both 295 and 4 K, plus their ratio, are plotted as a function of pressure in Figs. 3(a), 3(b) and 3(c), respectively. The disappearance of the resistivity knee in Fig. 2 near 8 GPa is accompanied by a peak in R(295 K), a sharp rise in R(4 K), and a sharp fall in their ratio. The steady climb in $R(T)$ upon releasing pressure seen in Fig. 3(a) arises from strong plastic deformation of the sample as the pressure cell expands.

As seen in the left inset to Fig. 2, the resistance at 0.9 GPa for temperatures up to ∼20 K can be described by the simple power law, $R(T) = R_o + AT^n$ with $n \simeq 1.8$, in agreement with that reported at ambient pressure [10]. With increasing pressure n increases to 1.9, 1.9, 2.0, and 2.0 at pressures 1.7, 2.8, 5.7, and 6.7 GPa, respectively. A value of n greater than 2 would point to spin-wave scattering contributions [10]. That $R(T)$ follows a simple quadratic temperature ($n = 2$) dependence under pressure is consistent with Fermi-liquid behavior where electron-electron scattering dominates (see right inset to Fig. 2).

The magnetic ordering temperature T_N was determined from the derivative dR/dT and is defined as the temperature where dR/dT has fallen halfway down from its maximum value to the plateau at higher temperatures. An example for this is shown in the inset to Fig. 3(d). As seen in Fig. 3(d), T_N increases strongly with pressure, in agreement with the results from Ref. [10] to 0.5 GPa. Such a stabilization of magnetic order under high pressure has been observed in other Heusler and semi-Heusler compounds [4,23,25–27].

B. X-ray diffraction

To explore whether a structural transition is responsible for the sudden change in $R(T)$ near 8 GPa seen in Fig. 2, high-pressure powder x-ray diffraction experiments were carried out. Under ambient conditions CuMnSb crystallizes in the cubic $C1_b$ semi-Heusler structure (space group $F\bar{4}3m$) with Cu at (0, 0, 0), Mn at (1/4, 1/4, 1/4), and Sb at (3/4, 3/4, 3/4) and $z = 4$, where z is number of formula units per unit cell. Angle dispersive x-ray diffraction measurements on polycrystalline samples were performed in two separate runs.

In the first experiment pressure was increased at room temperature to 36 GPa as shown in the Fig. 4. The initial cubic phase, identified by sharp Bragg peaks, was found to be stable to ∼7 GPa beyond which new peaks emerged in the diffraction pattern indicating a structural transition to a lower symmetry phase. At 7.5 GPa diffraction peaks from both phases coexist. This indicates the first-order nature of the structural transition. Above this pressure peaks from the cubic phase vanish completely and only the high-pressure phase remains. However, the peaks from the high-pressure phase are seen to be very broad. After pressure release the structure transformed back to the cubic phase. The significant peak broadening suggests that kinetic barriers at room temperature might prevent the completion of the transition to the high-pressure phase and hinder the unambiguous determination of its structure.

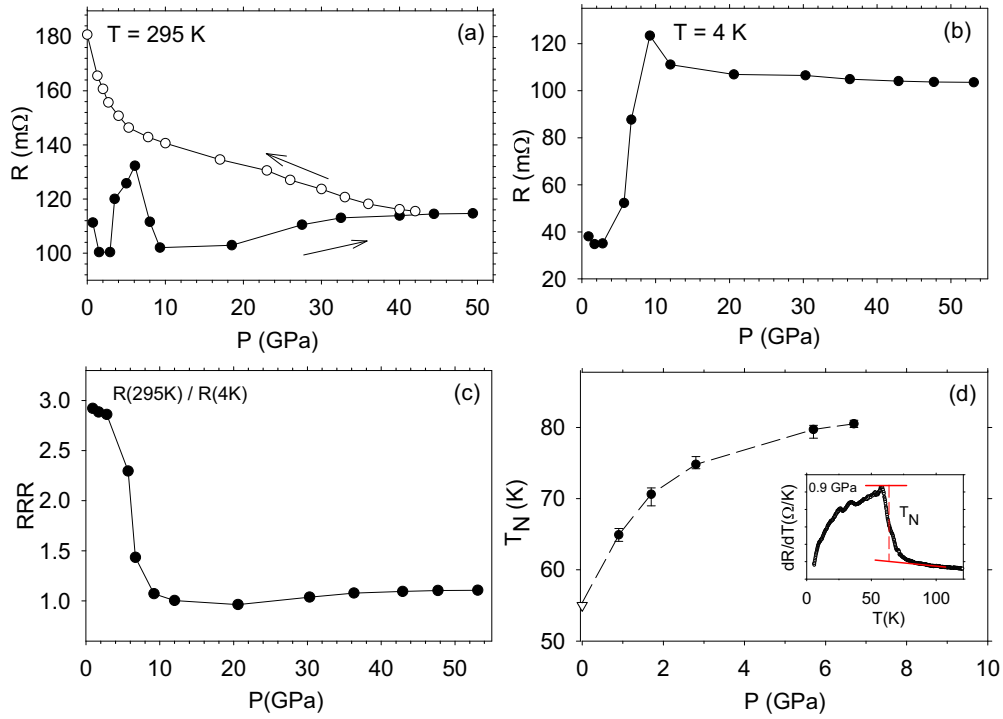

FIG. 3. As a function of pressure: (a) resistance at 295 K for increasing (•) and decreasing (○) pressure; (b) residual resistance at 4 K; (c) residual resistance ratio [RRR = $R(295\ \mathrm{K})/R(4\ \mathrm{K})$]; (d) antiferromagnetic transition temperature T_N—our data (•), data from Ref. [7] (▽) . Inset shows how T_N is determined from dR/dT using data at 0.9 GPa. In all graphs lines through data are guides to the eye.

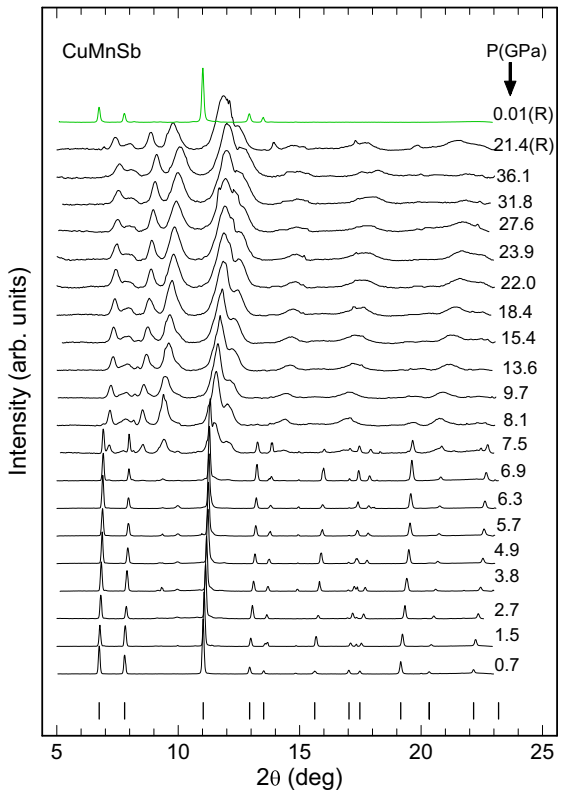

FIG. 4. X-ray diffraction patterns at various high pressures in run 1 at room temperature. "R" indicates released pressure.

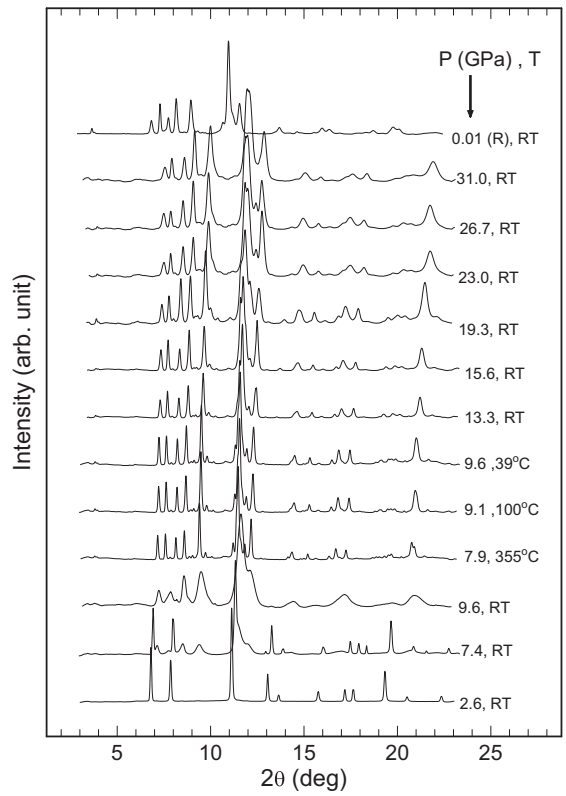

FIG. 5. X-ray diffraction patterns at representative high-pressure/high-temperature conditions in run 2. Order of measurement bottom to top. RT stands for "room temperature."

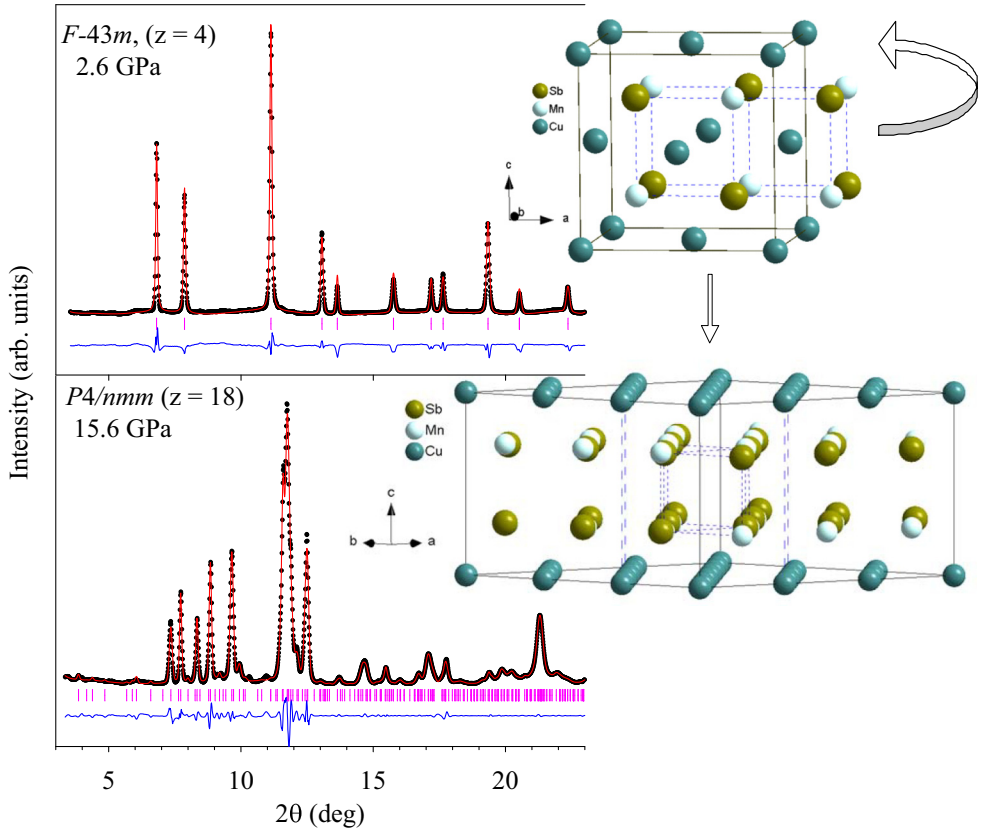

FIG. 6. Le Bail profile fitting of diffraction data at two different pressures, 2.6 and 15.6 GPa, from run 2 (top, cubic phase; bottom, tetragonal phase). Fitted spectra (red solid line), difference plot (blue solid line), and Bragg peak positions (tick marks) are shown. Right panel shows transformation from cubic to tetragonal structure.

As thermal energy is known to play a vital role in overcoming kinetic barriers, a second experiment was performed at high pressure and high temperature. Figure 5 shows the diffraction spectra at various *P-T* conditions. First, the pressure was increased at room temperature to 9.6 GPa, i.e., above the structural transition pressure. The high-pressure phase with broad peaks was observed again. Then at this pressure the temperature was raised to 355 °C. As the temperature increased, the pressure decreased from 9.6 GPa at room temperature to 7.9 GPa at 355 °C. After heat treating the high-pressure phase to temperatures as high as 355 °C for 30 min the diffraction pattern becomes appreciably sharper indicating the completion of the structural transition. This temperature is lower than the order-disorder transition temperature ∼480 °C reported for CuMnSb [2]. As the temperature was brought back to ambient, no spectral changes were observed during the cooling process.

After the heat treatment the peaks become better resolved with the clear appearance of weak low angle peaks near $2\theta = 4^{\circ}$, indicating longer unit cell dimensions. Pressure was then increased at room temperature to 31 GPa as shown in Fig. 5. The high-pressure phase is found to be stable up to 31 GPa and was retained on pressure release. The high-pressure phase can be indexed as the superstructure (cell tripling in *ab* plane) of Cu_2Sb-type tetragonal structure with space group $P4/nmm$ (129) and $z = 18$ [42]. The cubic to tetragonal transition in CuMnSb is found to be of the reconstructive type of first-order structural phase transition, as $P4/nmm$ is not a direct subgroup of $F\bar{4}3m$.

Due to the substantial texture in the XRD data, Rietveld refinement cannot be performed and we are unable to determine the type and concentration of dominant defects present in the sample. The structural parameters were extracted from Le Bail refinement. Figure 6 shows a typical Le Bail profile fitting for the low-pressure cubic phase and high-pressure tetragonal phase. The right panel illustrates the structure transformation mechanism from cubic to tetragonal. In the ambient pressure cubic phase, Mn and Sb atoms form a regular cube shown as dotted lines with a Cu atom at its center. In the high-pressure phase, the central layer of Cu atoms moves to the adjacent Cu planes. The arrow indicates the movement of Cu atoms from the middle layer to the top and bottom layers. The Mn-Sb cube gets distorted with a zigzag arrangement of Mn and Sb atoms.

The pressure dependence of the lattice parameters a_c, c_t, $\sqrt{2}a_t/3$, as well as the c/a ratio and equation of state are plotted in Fig. 7. The relevant crystallographic data for the cubic and tetragonal phases of CuMnSb are given in Table I. The $V(P)$ data were fitted with the third-order Birch-Murnaghan equation of state [43]. The fit yields for the cubic phase the bulk modulus $B_c = 58.2 \pm 1.7$ GPa and its derivative at zero pressure $B_c' = 9.6$. This value of the bulk modulus is somewhat lower than that calculated (78 GPa) for CuMnSb's cubic phase [44]. For the tetragonal phase the bulk modulus is $B_t = 138.5 \pm 3.2$ GPa

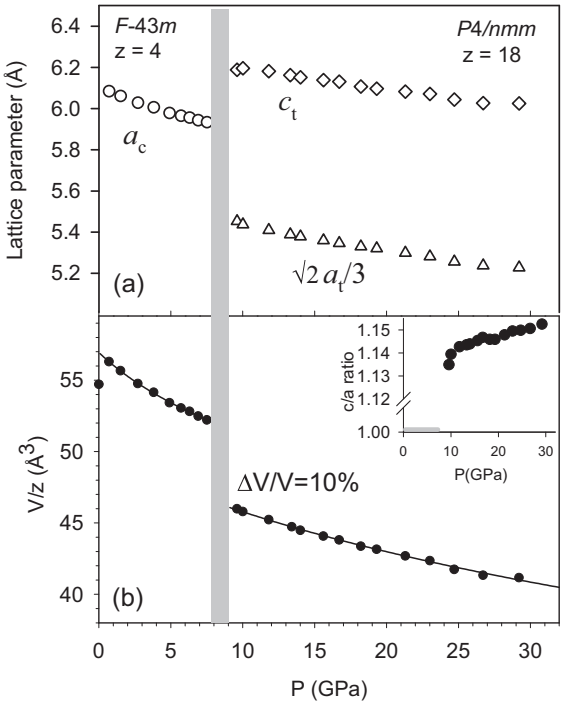

FIG. 7. (a) Lattice constants of CuMnSb as a function of pressure. (b) Unit cell volume versus pressure. Solid black lines show fitted Birch-Murnaghan equation of state. For high-pressure phase, data up to 23 GPa were used to fit equation of state. Inset gives the c/a ratio as a function of pressure.

with its derivative $B_t' = 4$ (fixed). The first-order transition is associated with a volume discontinuity of $\sim 10\%$ near 8 GPa.

C. Density functional theory

Density functional theory (DFT) calculations on CuMnSb were carried out with the projector augmented wave method, as implemented in the VASP package [45,46] within the local density approximation. For Cu $4s$ and $3d$, for Mn $3p$, $4s$, and $3d$, and for Sb $5s$ and $5p$ states were included as valence states. A plane-wave basis set with a cutoff energy of 400 eV is used. The first Brillouin zone integration was carried out with an $12 \times 12 \times 12$ Γ-centered Monkhorst-Pack mesh. For the ambient phase the AFM structure consists of alternating (111) planes of Mn atoms with aligned spins, and for the high-pressure phase the AFM structure consists of alternating (001) planes of Mn atoms with aligned spins, as reported for CuMnAs [29].

TABLE I. Crystallographic data for the cubic phase and the high-pressure tetragonal phase of CuMnSb obtained from Le Bail refinement.

P(GPa)	2.6 GPa	15.6 GPa
Space Group	$F\bar{4}3m$	$P4/nmm$
$a = b$ (Å)	6.028(1)	11.369(4)
c (Å)	6.028(1)	6.138(3)
V (Å^3)	219.09(2)	792.4(1)
z	4	18
B (GPa)	58.2 ± 1.7	138.5 ± 3.2
B'	9.6	4 (fix)
Atomic parameters		
Cu1	$4a$ (0,0,0)	$2a$ (0.75,0.25,0)
Mn1	$4c$ (0.25,0.25,0.25)	$2c$ (0.25,0.25,0.7275)
Sb1	$4d$ (0.75,0.75,0.75)	$2c$ (0.25,0.25,0.2971)
Cu2		$8g$ (0.4166,0.5833,0)
Mn2		$8i$ (0.25,0.5833,0.7275)
Sb2		$8i$ (0.25,0.5833,0.2971)
Cu3		$8i$ (0.25,0.4166,1)
Mn3		$8j$ (0.5833,0.5833,0.7275)
Sb3		$8j$ (0.5833,0.5833,0.2971)

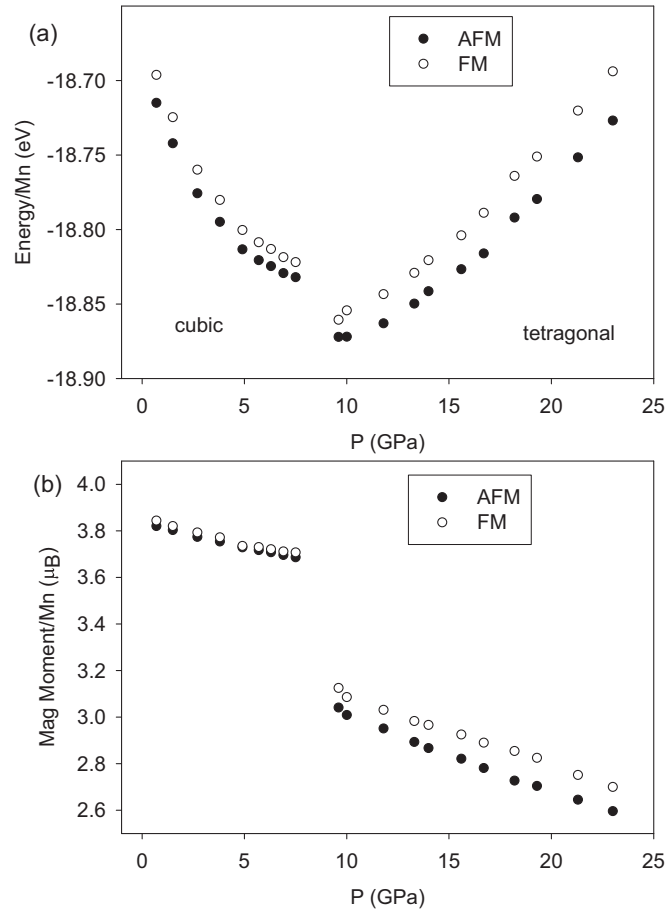

FIG. 8. Results of DFT calculations for CuMnSb in both cubic and tetragonal phases as a function of pressure. (a) Relative energies of FM and AFM phases. (b) Magnetic moment of Mn vs pressure.

Magnetic ordering is energetically favored over paramagnetism by approximately 1.6 eV (0.5 eV) in the cubic (tetragonal) structure. The calculated relative energies of the AFM and FM states as a function of pressure for both the cubic and tetragonal phases of CuMnSb are shown in Fig. 8(a). AFM order lies lowest in energy with the energy separation particularly large in the tetragonal phase. AFM order would thus be anticipated in the tetragonal phase. In Fig. 8(b) the calculated magnetic moment is seen to drop by $\sim 15\%$.

IV. DISCUSSION

The pressure dependence of the Néel temperature of the cubic semimetallic compound CuMnSb was determined by

resistivity measurements to 7 GPa. T_N increases rapidly with pressure from ∼50–83 K at 7 GPa. This is consistent with the interaction curve defined by Kanomata *et al.* [4] where the magnetic transition temperatures of a series of Heusler compounds are found to increase with decreasing nearest-neighbor Mn-Mn interatomic distance. A theoretical analysis by Şaşioğlu *et al.* [20] is able to account for this behavior in terms of the competition between two opposing trends, the stronger effect of the increasing carrier hopping compared with the effect of decreasing atomic moments.

The present DFT calculations on CuMnSb as a function of pressure agree with those of Jeong *et al.* [8] at ambient pressure and correctly account for the retention of AFM order throughout the cubic phase. This good agreement lends support to the DFT prediction that AFM order is retained in the tetragonal phase, particularly since its energy separation to ferromagnetism is significantly greater than in the cubic phase. The lowering of symmetry by the cubic-tetragonal phase transition near 8 GPa should remove magnetic frustration and thus possibly enable the magnetic ordering temperature in tetragonal CuMnSb to take on values well above ambient temperature, as are normally found for semi-Heusler and full Heusler compounds. The present results are consistent with this scenario since in the tetragonal phase no sign of the characteristic knee in $R(T)$ from magnetic ordering is observed in our subambient temperature range. However, we cannot exclude the possibility that T_N has dropped below the measured temperature range to 4 K. High-pressure neutron diffraction experiments are recommended to clarify the exact nature of the magnetic ordering and the temperature at which it occurs.

At first glance it might seem puzzling that the tetragonal phase is retained upon release of pressure in the resistivity measurements but not in the x-ray diffraction studies, both carried out at ambient temperature. The different pressure media used offer a likely explanation. In run 1 of the x-ray diffraction experiments the hydrostatic pressure medium neon was used. The broad diffraction lines above 8 GPa give evidence that the reconstructive cubic-to-tetragonal phase transition is not complete, likely due to kinetic barriers, leaving the high-pressure phase in a metastable state. Upon releasing the pressure it was thus relatively easy for the sample to revert back to the cubic phase. In the resistivity measurements, however, where nonhydrostatic cBN loaded epoxy served as pressure medium, substantial plastic deformation of the sample occurs as pressure is applied, leading to the buildup of several types of lattice defects and additional kinetic barriers unrelated to those naturally occurring in the course of the cubic-tetragonal phase transition. These additional kinetic barriers are likely responsible for the retention of the high-pressure tetragonal phase on release of pressure.

In contrast, in run 2 of the high-pressure x-ray diffraction experiment, the tetragonal phase is retained after pressure is released. In this experiment with neon pressure medium, the sample was first brought to the tetragonal phase at 9.5 GPa and then heated up to temperatures as high as 355 °C, whereby the diffraction peaks sharpened up dramatically, indicating the completion of the cubic-to-tetragonal phase transition. The elevated temperatures served to allow the sample to overcome the kinetic barriers so that the high-pressure tetragonal phase became thermodynamically stable. That the sample remained in the tetragonal phase upon release of pressure at room temperature indicates that the kinetic barriers had become too large in the stable tetragonal phase to allow the transition back to the cubic phase. The tetragonal phase was thus retained.

To summarize, we report magnetic and structural phase transitions of the AFM semi-Heusler compound CuMnSb as a function of pressure. The Néel temperature rises rapidly from the unusually low value ∼50–83 K at 7 GPa. Near 8 GPa a first-order structural transition to a tetragonal phase occurs with no sign in the temperature-dependent resistivity of a magnetic transition at subambient temperatures. It is likely that this transition to a lower symmetry tetragonal structure serves to remove the magnetic frustration responsible for the low value of the Néel temperature, potentially allowing it to shift to temperatures well above ambient. DFT calculations support this conclusion, revealing the dominance of the AFM phase in the high pressure tetragonal structure of CuMnSb.

ACKNOWLEDGMENTS

The experimental assistance of the HPCAT beamline scientists C. Park and S. Sinogelkin is gratefully acknowledged. Work at Washington University is supported by the National Science Foundation (NSF) through Grants No. DMR-1104742 and No. DMR-1505345 and by the Carnegie/U.S. Department of Energy Alliance Center (CDAC) through NNSA/DOE Grant No. DE-FC52-08NA28554. Financial support for the work at the Technical University of Munich was received from the Deutsche Forschungsgemeinschaft (DFG) TRR80 (projects E1 and F2). W.B. would like to acknowledge the partial support by COMPRES, the Consortium for Materials Properties Research in Earth Sciences under NSF Cooperative Agreement EAR 1606856. Portions of this work were performed at HPCAT (Sector 16), Advanced Photon Source (APS), Argonne National Laboratory. HPCAT operations are supported by DOE-NNSA under Award No. DE-NA0001974, with partial instrumentation funding by NSF. The Advanced Photon Source is a U.S. Department of Energy (DOE) Office of Science User Facility operated for the DOE Office of Science by Argonne National Laboratory under Contract No. DE-AC02-06CH11357.

[1] T. Graf, C. Felser, and S. S. P. Parkin, Simple rules for the understanding of Heusler compounds, Prog. Solid State Chem. **39**, 1 (2011).

[2] M. J. Otto, R. A. M. van Woerden, P. J. van der Valk, J. Wijngaard, C. F. van Bruggen, and C. Haas, Half-metallic ferromagnets: II. Transport properties of NiMnSb and related inter-metallic compounds, J. Phys.: Condens. Matter **1**, 2351 (1989).

[3] K. Watanabe, On new ferromagnetic intermetallic compounds PtMnSn and PtMnSb, J. Phys. Soc. Jpn. **28**, 302 (1970).

[4] See Fig 7 in T. Kanomata, K. Shirakawa, and T. Kaneko, Effect of hydrostatic pressure on the Curie temperature of the Heusler alloys Ni_2MnZ (Z = Al, Ga, In, Sn And Sb), J. Magn. Magn. Mater. **65**, 76 (1987).

[5] K. Endo, T. Ohoyama, and R. Kimura, Antiferromagnetism of CuMnSb, J. Phys. Soc. Jpn. **25**, 907 (1968).

[6] R. H. Forster, G. B. Johnston, and D. A. Wheeler, Studies on the Heusler alloys-III. The antiferro-magnetic phase in the Cu-Mn-Sb system, J. Phys. Chem. Solids **29**, 855 (1968).

[7] A. Regnat, A. Bauer, A. Senyshyn, M. Meven, K. Hradil, P. Jorba, K. Nemkovski, B. Pedersen, R. Georgii, S. Gottlieb-Schönmeyer, and C. Pfleiderer, Canted antiferromagnetism in phase-pure CuMnSb, Phys. Rev. Mater. **2**, 054413 (2018).

[8] T. Jeong, R. Weht, and W. E. Pickett, Semimetallic antiferromagnetism in the half-Heusler compound CuMnSb, Phys. Rev. B **71**, 184103 (2005).

[9] C. Pfleiderer, Are Mn_3Si and CuMnSb antiferromagnetic half-metals? Physica B **329-333**, 1085 (2003).

[10] J. Bœuf, C. Pfleiderer, and A. Faißt, Low-temperature properties of the semi-Heusler compound CuMnSb, Phys. Rev. B **74**, 024428 (2006).

[11] M. Doerr, J. Bœuf, C. Pfleiderer, M. Rotter, N. Kozlova, D. Eckert, P. Kerschl, K.-H. Müller, and M. Loewenhaupt, Search for half-metallic antiferromagnetism using pulsed magnetic fields: Experimental investigation of Mn_3Si, CuMnSb, and PdMnTe, Physica B **346-347**, 137 (2004).

[12] M. J. Otto, R. A. M. van Woerden, P. J. van der Valk, J. Wijngaard, C. F. van Bruggen, C. Haas, and K. H. J. Buschow, Half-metallic ferromagnets: I. Structure and magnetic properties of NiMnSb and related inter-metallic compounds, J. Phys.: Condens. Matter **1**, 2341 (1989).

[13] F. Máca, J. Kudrnovsky, V. Drchal, I. Turek, O. Stelmakhovych, P. Beran, A. Llobet, and X. Marti, Defect-induced magnetic structure of CuMnSb, Phys. Rev. B **94**, 094407 (2016).

[14] K. Endo, Magnetic studies of Cl_b-compounds CuMnSb, PdMnSb and $Cu_{1-x}(Ni\text{ or }Pd)_xMnSb$, J. Phys. Soc. Jpn. **29**, 643 (1970).

[15] S. K. Ren, Y. X. Wang, Y. J. Zhang, G. B. Ji, F. M. Zhang, and Y. W. Du, Magnetic and electrical properties of the half-Heusler $Cu_xNi_{1-x}MnSb$ alloys, J. Alloys Compd. **387**, 32 (2005).

[16] M. Halder, S. M. Yusuf, A. Kumar, A. K. Nigam, and L. Keller, Crossover from antiferromagnetic to ferromagnetic ordering in the semi-Heusler alloys $Cu_{1-x}Ni_xMnSb$ with increasing Ni concentration, Phys. Rev. B **84**, 094435 (2011).

[17] E. Şaşioğlu, L. M. Sandratskii, and P. Bruno, Role of conduction electrons in mediating exchange interactions in Mn-based Heusler alloys, Phys. Rev. B **77**, 064417 (2008).

[18] I. Galanakis, E. Şaşioğlu, and K. Özdoğan, Magnetic phase transition in half-metallic CoMnSb and NiMnSb semi-Heusler alloys upon Cu doping: First-principles calculations, Phys. Rev. B **77**, 214417 (2008).

[19] E. Şaşioğlu, L. M. Sandratskii, and P. Bruno, Magnetic phase diagram of the semi-Heusler alloys from first principles, Appl. Phys. Lett. **89**, 222508 (2006).

[20] E. Şaşioğlu, L. M. Sandratskii, and P. Bruno, Pressure dependence of the Curie temperature in Ni_2MnSn Heusler alloy: A first-principles study, Phys. Rev. B **71**, 214412 (2005).

[21] S. K. Bose, J. Kudrnovsky, V. Drchal, and I. Turek, Pressure dependence of Curie temperature and resistivity in complex Heusler alloys, Phys. Rev. B **84**, 174422 (2011).

[22] I. Tutic, J. Herran, B. Staten, P. Gray, T. Paudel, A. Sokolov, E. Tsymbal, and P. Lukashev, Effects of pressure and strain on spin polarization of IrMnSb, J. Phys.: Condens. Matter **29**, 075801 (2017).

[23] S. Kyuji, S. Endo, T. Kanomata, and F. Ono, Pressure dependence of the Curie temperature in Ni_2MnSn Heusler alloy, Physica B **237-238**, 523 (1997).

[24] C. Salazar Mejía, K. Mydeen, P. Naumov, S. A. Medvedev, C. Wang, M. Hanfland, A. K. Nayak, U. Schwarz, C. Felser, and M. Nicklas, Suppression of the ferromagnetic order in the Heusler alloy $Ni_{50}Mn_{35}In_{15}$ by hydrostatic pressure, Appl. Phys. Lett. **108**, 261903 (2016).

[25] I. G. Austin and P. K. Mishra, The effect of pressure on the Curie temperature and resistivity of some rare-earth metals and Heusler alloys, Philos. Mag. **15**, 529 (1967).

[26] A. G. Gavriliuk, G. N. Stepanov, V. A. Sidorov, and S. M. Irkaev, Hyperfine magnetic fields and Curie temperature in the Heusler alloy Ni_2MnSn at high pressure, J. Appl. Phys. **79**, 2609 (1996)

[27] Y. Chieda, T. Kanomata, K. Fukushima, K. Matsubayashi, Y. Uwatoko, R. Kainuma, K. Oikawa, K. Ishida, K. Obara, and T. Shishido, Magnetic properties of Mn-rich Ni_2MnSn Heusler alloys under pressure, J. Alloys Compd. **486**, 51 (2009).

[28] F. Máca, J. Mašek, O. Stelmakhovych, X. Martí, H. Reichlová, K. Uhlířová, P. Beran, P. Wadley, V. Novák, and T. Jungwirth, Room-temperature antiferromagnetism in CuMnAs, J. Magn. Magn. Mater. **324**, 1606 (2012).

[29] P. Wadley, V. Novák, R. P. Campion, C. Rinaldi, X. Martí, H. Reichlová, J. Železný, J. Gazquez, M. A. Roldan, M. Varela, D. Khalyavin, S. Langridge, D. Kriegner, F. Máca, J. Mašek, R. Bertacco, V. Holý, A. W. Rushforth, K. W. Edmonds, B. L. Gallagher, C. T. Foxon, J. Wunderlich, and T. Jungwirth, Tetragonal phase of epitaxial room-temperature antiferromagnet CuMnAs, Nat. Commun. **4**, 2322 (2013).

[30] P. Wadley, B. Howells, J. Železný, C. Andrews, V. Hills, R. P. Campion, V. Novák, K. Olejník, F. Maccherozzi, S. S. Dhesi, S. Y. Martin, T. Wagner, J. Wunderlich, F. Freimuth, Y. Mokrousov, J. Kuneš, J. S. Chauhan, M. J. Grzybowski, A. W. Rushforth, K. W. Edmonds, B. L. Gallagher, and T. Jungwirth, Electrical switching of an antiferromagnet, Science **351**, 587 (2016).

[31] A. Neubauer, J. Bœf, A. Bauer, B. Russ, H. v. Löhneysen, and C. Pfleiderer, Ultra-high vacuum compatible image furnace, Rev. Sci. Instrum. **82**, 013902 (2011).

[32] A. Bauer, G. Benka, A. Regnat, C. Franz, and C. Pfleiderer, Ultra-high vacuum compatible preparation chain for intermetallic compounds, Rev. Sci. Instrum. **87**, 113902 (2016).

[33] A. Bauer, A. Neubauer, W. Münzer, A. Regnat, G. Benka, M. Meven, B. Pedersen, and C. Pfleiderer, Ultra-high vacuum compatible induction-heated rod casting furnace, Rev. Sci. Instrum. **87**, 063909 (2016).

[34] J. S. Schilling, Magnetism at high pressure, in *Proceedings of the 9th AIRAPT International High Pressure Conference, Albany, New York, July 24–29, 1983*, edited by C. Homan, R. K. MacCrone, and E. Whalley (North-Holland, New York, 1984); Mat. Res. Soc. Symp. Proc. **22**, 79 (1984).

[35] A. D. Chijioke, W. J. Nellis, A. Soldatov, and I. F. Silvera, The ruby pressure standard to 150 GPa, J. Appl. Phys. **98**, 114905 (2005).

[36] J. Lim, G. Fabbris, D. Haskel, and J. S. Schilling, Magnetic ordering at anomalously high temperatures in Dy at extreme pressures, Phys. Rev. B **91**, 045116 (2015).

[37] K. Shimizu, K. Amaya, and N. Suzuki, Pressure-induced superconductivity in elemental materials, J. Phys. Soc. Jpn. **74**, 1345 (2005).

[38] O. L. Anderson, D. G. Isaak, and S. Yamamoto, Anharmonicity and the equation of state for gold, J. Appl. Phys. **65**, 1534 (1989).

[39] A. Hammersley, *Computer program* FIT2D (ESRF, Grenoble, 1998).

[40] A. C. Larson and R. B. Von Dreele, GSAS general structure analysis system, Los Alamos National Laboratory Report No. LAUR 86-748, 2000.

[41] W. H. Schreiner and D. E. Brandao, Electrical resistivity of the $C1_b$ alloy CuMnSb, Solid State Commun. **43**, 463 (1982).

[42] J. Nuss and M. Jansen, Zur abgrenzung der PbFCl- und Cu_2Sb-strukturfamilien: Neubestimmung und verfeinerung der kristallstrukturen von CuMgSb, Cu_2Sb und CuMgAs, Z. Anorg. Allg. Chem. **628**, 1152 (2002).

[43] F. Birch, Finite strain isotherm and velocities for single crystal and polycrystalline NaCl at high pressures and 300 K, J. Geophys. Res. **83**, 1257 (1978).

[44] S. Palaz, H. Koc, H. Ozisik, E. Deligoz, A. M. Mamedov, and E. Ozbay, Optical and magnetic properties of some XMnSb and Co_2YZ compounds: *ab initio* calculations, Phys. Status Solidi C **14**, 1600182 (2017).

[45] G. Kresse and J. Furthmüller, Efficient iterative schemes for *ab initio* total-energy calculations using a plane-wave basis set, Phys. Rev. B **54**, 11169 (1996).

[46] G. Kresse and D. Joubert, From ultrasoft pseudopotentials to the projector augmented-wave method, Phys. Rev. B **59**, 1758 (1999).